Physica D 240 (2011) 131–139

Contents lists available at ScienceDirect

Physica D

journal homepage: www.elsevier.com/locate/physd

Instability and freezing in a solidifying melt conduit

Miranda C. Holmes-Cerfon [a,*], J.A. Whitehead [b]

[a] Courant Institute of Mathematical Sciences, New York, NY 10012, USA
[b] Woods Hole Oceanographic Institution, Woods Hole, MA, USA

ARTICLE INFO

Article history:
Available online 13 November 2010

Keywords:
Melt conduits
Fluid dynamics
Solid/melt interface
Stability analysis
Magma
Viscous fluid

ABSTRACT

Previous works have shown that when liquid flows in a pipe whose boundary temperature is below freezing, a tubular drainage conduit forms surrounded by solidified material that freezes shut under the appropriate combination of forcing conditions. We conduct laboratory experiments with wax in which the tube freezes shut below a certain value of flux from a pump. As the flux is gradually decreased to this value, the total pressure drop across the length of the tube first decreases to a minimum value and then rises before freezing. Previous theoretical models of a tube driven by a constant pressure drop suggest that once the pressure minimum is reached, the states for a lower flux should be unstable and the tube should therefore freeze-up. In our experiments, flux and pressure drop were coupled, and this motivates us to extend the theory for low Reynolds number flow through a tube with solidification to incorporate a simple pressure-drop–flux relationship. Our model predicts a steady-state relationship between flux and pressure drop that has a minimum pressure as the flux is varied. The stability properties of these steady states depend on the boundary conditions: for a fixed flux, they are all stable, whereas for fixed pressure drop, only those with a flux larger than that at the pressure drop minimum are stable. For a mixed pressure–flux condition, the stability threshold of the steady states lies between these two end members. This provides a possible mechanism for the experimental observations.

1. Introduction

Injected liquids that freeze as they flow are common in many areas of engineering (injection molding, freezing, metallurgy) as well as in earth and planetary sciences (lava tubes, magma conduits, glaciology, and magma fissure flows). In such cases, liquid flows through a region whose boundary temperature is below the solidification temperature of the liquid, so that advection of heat by the warm liquid acts in tandem with removal of heat by the boundary. In some cases, the cooling is weak enough that solid may form at the boundary but leave a central melted tube where liquid flows. In other cases the entire body of liquid may freeze so that all flow ceases. It is useful to know the conditions that are necessary for such freezing.

In the geophysical literature, the pioneering study of the dynamics of melting and solidifying material was for flow up a fissure with variable gap width [1,2], where conditions for melt-back (widening) or solidification (narrowing) of the gap are calculated from thermal energy budgets. This was followed by many studies on the dynamics of either fissure flow or lava dynamics, investigating situations such as the temperature distribution and velocity profile in a magma tube, or the driving pressure required to keep it open (e.g. [3–6]). These studies invariably use simplified, time-independent geometries for the tube boundary, and generally, little analysis has been made of the stability of the flows. A notable exception is the theoretical study by Lister and Dellar [7], in which cooling occurs at infinity and therefore no steady-state tube is possible.

For engineering purposes, numerous studies focus on flow of a liquid in a container whose walls are below the freezing temperature. Applications include injection molding, the freezing of water, the condensation of water vapor in ducts, and metal casting, among others. For example, experiments with water demonstrate the focusing of flow into a narrow region along with the formation of waves of solid on the walls, and in some cases freeze-up [8–11]. A common feature is that the curve of steady-state pressure drop against flux exhibits sizeable curvature, in many cases reaching a minimum such that as the flux is gradually decreased, the pressure drop first decreases, then increases, a result that has been recovered in theoretical studies [8,12]. If the flow is driven by imposing a fixed pressure drop, however, the low-flux branch of this curve, where pressure drop increases with decreasing flux, is unstable: a perturbation making a smaller cross-sectional area produces more drag, which produces slower flow that leads to colder liquid and more solidification and finally to total freezing [13,14]. If, instead, the flow is driven by a pump imposing a fixed flux, the steady state is presumed to be stable, although a complete stability

* Corresponding address: Harvard University, School of Engineering and Applied Science, Cambridge, MA 02138, USA.
E-mail address: mholcer@seas.harvard.edu (M.C. Holmes-Cerfon).

0167-2789/$ – see front matter © 2010 Elsevier B.V. All rights reserved.
doi:10.1016/j.physd.2010.10.009

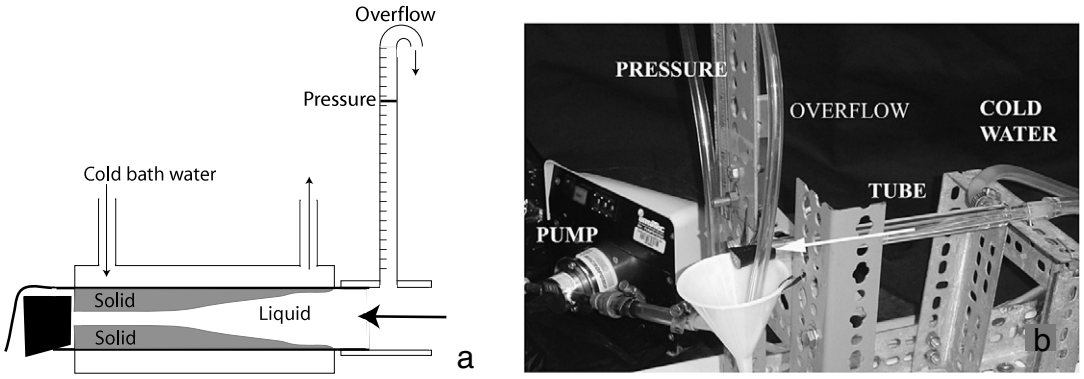

Fig. 1. (a) Sketch of the tube surrounded by water from a cold bath. The wax enters from the right and solidifies (grey) at the outer radius of the liquid tube. Upstream liquid elevation indicates the pressure. (b) A photograph of the apparatus.

analysis has never been done; a smaller cross-sectional area makes a faster flow that brings warmer fluid from upstream to the region, which widens the perturbation. The constant flux upstream condition is widely used in theories that calculate the solid accumulation along flow ducts of assorted material properties and shapes (e.g., [9,15,16]), but such problems do not exhibit flow freeze-up from an instability.

Since theory shows that stability depends on the particular type of flow boundary condition that is imposed at the upstream end, our attention here is focused upon the stability of solidifying flow with a more general upstream condition than either constant flux or constant pressure drop. We tackle the question of stability with both experiment and theory. First, we describe laboratory experiments of flow through a pipe whose temperature is held below the solidus, in which there was a coupling between flux and pressure drop (Section 2). The flow froze when the steady-state flux was below a certain value. As the steady-state flux was decreased in successive experiments to this value, the pressure drop across the tube reached a minimum and then increased before freeze-up. This result is not explained by either constant flux or constant pressure drop models, one of which suggests freeze-up should never occur, and the other that it should occur as soon as the pressure minimum is reached. It motivates us to investigate the stability of low Reynolds number flow through a tube using a standard idealized theoretical model with the addition of a mixed pressure–flux upstream driving condition (Section 3). Essentially, we suppose the tube drains from an upstream reservoir into which fluid is pumped at a constant rate, so the total amount of fluid in the reservoir determines the driving pressure and therefore the flux through the tube. Naturally, this new upstream condition is intended to be a more realistic model both of conditions in our experiment as well as in some types of geological melt conduits, and possibly in some engineering applications. A linear stability analysis shows that the mixed upstream condition allows the stable range of the flow to extend to lower values of flux that are unstable for fixed pressure drop. Thus, it is in qualitative accord with the laboratory results. In addition, the theory predicts an oscillatory instability that has not been found in the previous theoretical studies. Numerical simulations recover both the new features (Section 3.4). In Section 3.5 we show how the basic model (without the stability results) can be used straightforwardly to provide a realistic constraint on the length of geological melt conduits.

The central implication of these results is that stability is very sensitive to the upstream conditions that drive the melt through the tube. This sensitivity may be one mechanism behind the complex nature of many real solidifying flows in nature and industry.

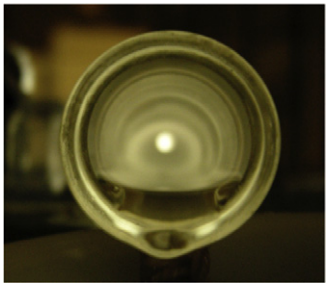

Fig. 2. A view looking upstream into the end of the melted tube. The melt fills the white circular region. The solid possesses circular rings of unknown origin.

2. Experiments with freezing of flow through a tube

We performed experiments with flow through a chilled circular pipe, whose setup is shown in Fig. 1. The pipe was a standard glass condenser for a chemistry laboratory with a central glass pipe of radius $r_0 = 0.49 \times 10^{-3}$ m surrounded by a sleeve (see Table 1 for list of symbols). The length of the portion of the pipe surrounded by this sleeve was $L = 0.18$ m. The sleeve was flushed with water from a constant temperature bath at temperature T_0 that was accurate to ± 0.1 °C. The central axis of the condenser was placed horizontally. Liquid at 20 °C was fed from a constant displacement metered pump into one end of the condenser. The pump volume flux rate (henceforth simply called either flux or, in case of a pump setting, the pumping rate) was calibrated to $\pm 2\%$. The other end was the tube exit fitted with a rubber stopper with a flat notch cut along the top. The liquid exited the glass tube by flowing over this notch; therefore, the stopper served as a miniature dam so that the pipe within the condenser remained filled with liquid at all times with no air traveling upstream from the exit into the tube. A photograph of the outlet with the stopper removed after a run shows a circular drainage channel surrounded by solid (Fig. 2). The ridges in the solid are evidence of uneven solidification whose origin will not be studied further here. The liquid was 1-Octadecene (Chevron Phillips C18, kindly donated). In this study, we simply call this material a wax. The freezing point (solidus temperature) is $T_s = 17.8$ °C and the pour point is half a degree higher at 18.3 °C, indicating that viscosity increases greatly close to the solidus. The specifications for the liquid state are: a thermal conductivity of $k = 0.114$ W/m K, a specific heat of $c_p = 2.26 \times 10^3$ j/kg K with significant changes in value near freezing temperature [17], a density of $\rho = 785$ kg/m^3 (these three give a thermal diffusivity of $\kappa = 0.64 \times 10^{-7}$ m^2 s^{-1}) and kinematic viscosity values of $\nu = 8.28 \times 10^{-6}$ m^2 s^{-1} at 31 °C and $\nu = 3.8 \times 10^{-6}$ m^2 s^{-1}

Table 1
List of symbols. For perturbation theory, the basic state is denoted by subscript 0 and the perturbation by subscript 1.

A	Upstream reservoir cross-sectional area
A_n	Coefficients of temperature solution
E	Radial heat flux in the solid
G_n	Coefficients of solution for flux of temperature $A_n\phi_n'(1)$
H	Elevation of liquid upstream of the tube
I	Radial heat flux in the liquid
L	Tube length
L_H	Latent heat of solidification
P	Pressure
ΔP	Pressure drop across entire tube
Pr	Prandtl number
Q	Volume flux through the tube
Q_i	Volume flux into upstream reservoir
S	Stefan number $L_H/C_p\,(T_i - T_s)$
T	Temperature in the liquid
T_e	Temperature in the solid
T_i	Temperature of fluid at inlet
T_n	Dimensionless temperature constant, equal to $(T_s - T_0)/(T_i - T_s)$
T_0	Temperature at the outer radius
T_s	Temperature of solidification
a	Radius of the solid–liquid interface
c_p	Specific heat
g	Acceleration of gravity
k	Thermal conductivity
p	Dimensionless pressure
Δp	Dimensionless pressure drop $r_0^4\Delta P/4\mu\kappa L^2$
$\Delta p_c\,(T_n)$	Critical value of pressure drop, below which no steady-state tube is possible
q	Dimensionless flux $2Q/\kappa\pi L$
q_i	Dimensionless inlet flux $2Q_i/\kappa\pi L$
$q_c(T_n)$	Critical value of flux, at which $\Delta p = \Delta p_c$
r	Radial coordinate
r_0	Outer tube radius
t	Time
u	Fluid velocity
u'	Dimensionless fluid velocity
v	Velocity in a radial direction
x	Coordinate along the axis of the tube
α	Dimensionless radius of solid–liquid interface a/r_0
ε	Amplitude of perturbation
η	Dimensionless radial coordinate r/a
θ	Dimensionless liquid temperature $(T - T_0)/(T_i - T_s)$
θ_e	Dimensionless temperature of solid $(T_e - T_0)/(T_i - T_s)$
κ	Thermal diffusivity $k/\rho c_p$
λ_n	Eigenvalues of the Graetz problem
μ	Dynamic viscosity
ν	Kinematic viscosity μ/ρ
ρ	Density
τ	Pressure–time constant $\pi S r_0^6\rho g/8A\mu\kappa L$
ϕ_n	Eigenvectors of the Graetz problem
χ	Dimensionless coordinate along axis x/L

at 37.8 °C. Also, the fluid is very hygroscopic. Since the model developed in subsequent sections assumes constant material properties, the fact that viscosity and specific heat changes greatly in the temperature range of interest means that we will only be able to compare the experimental results with prediction qualitatively.

For all experiments, the temperature of the liquid pumped into the condenser was $T_i = 20$ °C. After starting the liquid pump, the temperature of the water flushing the sleeve was set to a value below the solidus so that the wax became solid along the inner radius of the glass pipe as sketched in Fig. 1, with flow occurring in a central liquid tube. The liquid tube radius varied in the flow direction and it was a function of the pumping rate and sleeve temperature. We measured pressure immediately upstream of the condenser by splitting the upstream plastic tubing with a Y connection. The tube on one side of the Y was the input to the condenser and the other plastic tube was held vertically next to a centimeter scale to allow a measurement of pressure of the upstream fluid. Since pressure at the downstream end was fixed at atmospheric pressure, the elevation of the liquid surface in the vertical plastic tube above the elevation of the outlet was proportional to pressure drop across the condenser. This elevation was read to a precision of 1 mm. The vertical tube is also a storage region for liquid supplied by the pump. In fact, the difference between the flux of the pump and the flux out through the condenser is proportional to the rate of change of height in the vertical pressure tube. This provides a mixed pressure–flux upstream boundary condition to the flow through the condenser. The exact expression for this will be derived in the next section.

The top of the vertical plastic tube was bent over and extended back to the wax reservoir as an overflow. If upstream pressure became too great, the overflowing liquid indicated freeze-up of the tube.

The procedure for these experiments at the beginning of each day was to start with everything at room temperature so the wax was completely liquid. A run commenced by turning on the wax pump to a desired pumping rate and then changing the cold bath temperature from 20 °C to the desired value, which we call T_0. After about 15 min, the wax solidified along the inner radius of the tube and the flow continued through the liquid tube. The elevation in the vertical tube was measured many times until the value was steady, and then the final value of pressure (in units of vertical elevation) was recorded. The flux was also measured then.

Fig. 3 shows the elevation of the liquid surface in the vertical tube versus the imposed pumping rate, or flux for many runs in experiments with cold bath temperatures set to two different values: $T_0 = 5.0$ °C and $T_0 = 10.0$ °C. At both temperatures the flowing liquid froze shut at a pumping rate approximately 5% below the measurement on the extreme left. To the right of the freezing point, the inverse relation between the pressure and pumping rate was unmistakable. For $T_0 = 10.0$ °C, pressure increased slightly with pumping rate for flux $Q_i > 0.5 \times 10^{-6}$ m^3 s^{-1} but for $T_0 = 5.0$ °C, a pressure increase with flux is not visible. The errors for the pressure measurement and for the calibration of the pumping rate are approximately the size of the symbols. Since obviously the scatter about a smooth curve for all the data is considerable, we concluded after careful checking that the scatter is not from errors in measurement. In addition, we conducted long runs to determine whether the scatter was due to the experiment duration being too short. For all these experiments (which were conducted for more than two hours each, and compromise 70% of the data points), such scatter persisted even though the pressure reading had been constant for the entire second hour. Therefore, we believe the scatter is a basic feature and the scatter might possibly be due to small differences in the detailed shape of each frozen solid. In support of this, Fig. 2 shows irregularities in the solid surface near the exit.

The experiment results are scaled by noting that the experimental flow tube has the following variables: the glass tube radius r_0, tube length L, fluid viscosity μ, fluid density ρ, fluid thermal diffusivity κ, temperature at the inlet T_i, temperature of the surface of the tube T_0, temperature of solidus T_s, and flux of the liquid initially entering upstream Q_i. This totals 9 variables with four units: temperature, force, length and time. Therefore, five dimensionless numbers are needed. Two of them are simply temperature ratios, but they are best combined and expressed as $T_n = \frac{T_s - T_0}{T_i - T_s}$. A third is aspect ratio of the tube r_0/L. A fourth is Prandtl number $Pr = \nu/\kappa$, and the last is non-dimensional flux $q_i = \frac{2}{\kappa\pi L}Q_i$. In addition, we calculate a value of non-dimensional pressure drop $\Delta P = \frac{r_0^4}{4\mu\kappa L^2}P$, where P is the pressure above atmosphere pressure at the upstream end.

Using the values for this liquid, the Prandtl number is $Pr = 129$. Using the tube length and radius, and using the magnitude for flux near the minimum of about $Q_i = 0.3 \times 10^{-6}$ m^3 s^{-1} from Fig. 3, we get $q_i = 15$. The magnitude of scaled pressure from the same figure is found using the hydrostatic equation for pressure $P = \rho g H$, where acceleration from gravity is g and a typical elevation of

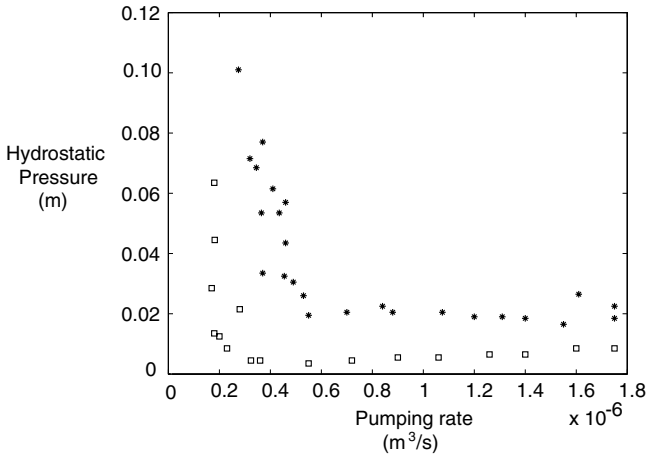

Fig. 3. Measured pressure versus flow rate with bath temperatures of 5.0 °C (stars) and 10.0 °C (squares), for experiments discussed in Section 2.

wax in the vertical pressure measuring tube is $H = 0.02$m. From this, we get $\Delta P = 1650$.

Next, the values of actual critical fluxes for freezing were checked by four precise experiments at four different values of $T_0 = 2.5, 5.0, 7.5$, and 10.0 °C. For each of these values, an experimental run started with the pump set at a value that allowed continuous flow. Then, the freezing point was approached by decreasing the pumping rate by 5% increments and waiting an hour or more to see if the flow froze. If the flow did not freeze after that time interval, another decrease was made. The aggregate time for each run was many hours. The lowest values of pumping rate at the above four temperature settings are 0.42, 0.23, 0.18, and 0.16×10^{-6} m^3 s^{-1}, successively, These correspond to non-dimensional values of $q_i = 23.2$, 12.7, 9.95, and 8.84 at $T_n = 6.95$, 5.82, 4.68, and 3.55, respectively. Flow ceased by freezing shut for incrementally changed pumping rates that were approximately 5% below these rates.

In experiments using more than the 5% incremental decrease in pumping rate from one experiment to the next, the critical flux for freezing was measurably larger. For example, the wax always froze shut for experiments at $T_0 = 10$ °C with a steady pumping rate of 0.36×10^{-6} m^3 s^{-1} and then after steady flow developed were given a 33% decrease in pumping rate to 0.24×10^{-6} m^3 s^{-1} ($q_i = 19.89$ to 13.26). The exact reason why a large incremental decrease leads to a higher critical flux than the value with a 5% incremental decrease, which in this case is 0.16×10^{-6} m^3 s^{-1} ($q_i = 8.84$), is unknown. Possibly the upstream pressure cannot build up rapidly enough to allow sufficient flux through the melt region when the interior radius shrinks.

After a steady flow developed, the stopper at the exit was removed to view the inner conduit radius by looking into the end of the pipe. A light beam from a slide projector at right angle to the tube and directed at the end of the tube far from the camera illuminated fluid upstream as the white circle in Fig. 2. Regrettably, we are skeptical about using such images to attempt to measure the diameter of the liquid conduit. Clearly, there was large distortion of the light as it passed to the camera across the curved liquid/air surface. Also, each light beam reaching the camera from the inside of the liquid tube was bent by the axial temperature distribution within the liquid tube with the axial equivalent of the mirage effect. Therefore, no optical measurements of the tube radius as a function of flow rate and sleeve temperature were attempted.

If the flux and the bath temperature were slightly above the values that gave freezing, the flow was easily made to freeze even with very small disturbances. For example, with a sleeve temperature of 2.5 °C, and pumping rate of 0.42×10^{-6} mm^3 s^{-1}, when the pump was stopped for five seconds, the flow ceased and never started again. Conversely, with the same initial conditions the flow resumed most of the time if the pump was stopped for three seconds, and it always resumed if the pump was stopped for only one second. We also found that a piece of very fine copper wire inserted into the liquid hole readily nucleated a freezing event.

3. Flow through a tube: theory

3.1. Fundamental equations

We begin the analysis by reviewing a standard theoretical model for a melt conduit of flow at low Reynolds number into a long cold pipe (e.g. [8]). The pipe has a fixed length L in the x-direction and it has a perfectly circular cross-section with constant radius r_0 (Fig. 4). Liquid enters the pipe at a uniform initial hot temperature T_i and it flows with laminar flow. The boundary of the pipe is maintained at a constant temperature T_0 that is colder than the solidification temperature T_s. The temperature varies continuously from $T = T(0, x, t) > T_s$ in the liquid at the center of the tube, to T_0 at r_0. Solid material forms a tube of radius $a(x, t)$ at the isotherm $T = T_s$.

A number of assumptions are made to make the model analytically tractable. A full list can be found in [8], but we mention those that will be most important. First, the basic flow is made as simple as possible by assuming that there are constant material properties, a simple cutoff solidification temperature, and no buoyancy force. Second, the Reynolds number is small enough for there to be no turbulence and no inertia in the momentum equation. Third, the length L is assumed to be large enough compared to r_0 that changes in the along-tube direction x are slow. Finally, the Stefan number is assumed to be large, so that the solidification process and corresponding motion of the crust are much slower than the thermal, advective, or viscous timescales. Therefore time derivatives are only retained in the equation for the radius, and while other fluid variables are time dependent, they are

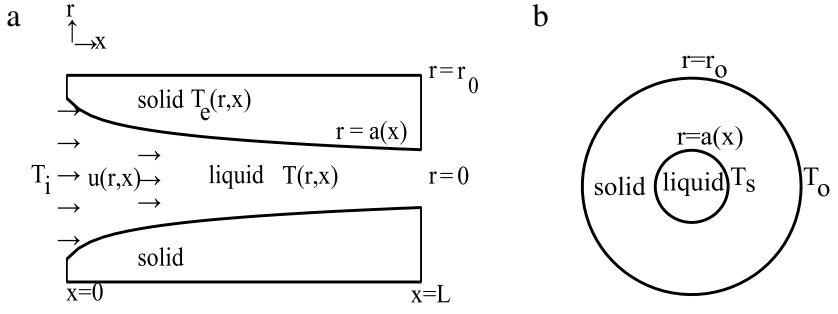

Fig. 4. (a) Cross-section through the centerline of the melt tube. (b) Cross-section tube across the direction of flow.

only quasi-steadily so via their dependence on the radius. We now proceed to introduce the basic equations.

The velocity in the downstream direction is given by the well-known equation for flow at low Reynolds number (e.g. [18]), $\frac{\partial P}{\partial x} = \mu \frac{1}{r}\frac{\partial}{\partial r}\left(r\frac{\partial u}{\partial r}\right)$, where $\partial P/\partial x$ is the pressure gradient in the axial direction, u is the velocity in the axial direction, μ is the fluid viscosity and r is the radial coordinate. The radial velocity v can be found from the condition of non-divergence, and is non-zero because the radius of the tube changes in the flow direction. The solution for u with the boundary condition $u = 0$ at $r = a(x,t)$ is Poiseuille flow $u = -\frac{\partial P}{\partial x}\frac{(a^2-r^2)}{4\mu}$. Integrating over the area determines the flux Q whose relation to the pressure gradient is

$$\frac{\partial P}{\partial x} = -\frac{8\mu Q}{\pi a^4}, \tag{3.1}$$

so the velocity can also be written as

$$u = \frac{2Q}{\pi a^2}\left(1-(r/a)^2\right). \tag{3.2}$$

In the solid, the temperature field T_e satisfies a diffusion equation when the x derivatives and time derivatives are neglected:

$$\frac{1}{r}\frac{\partial}{\partial r}\left(r\frac{\partial T_e}{\partial r}\right) = 0, \tag{3.3}$$

with the boundary conditions $T_e|_{r=r_0} = T_0$, $T_e|_{r=a} = T_s$. This can be solved to give

$$T_e = \frac{T_0 - T_S}{\ln\frac{r_0}{a}}\ln\frac{r}{a} + T_S. \tag{3.4}$$

In the liquid, the temperature field is determined by a balance between advection and diffusion when time derivatives are neglected:

$$u\frac{\partial T}{\partial x} + v\frac{\partial T}{\partial r} = \kappa\frac{1}{r}\frac{\partial}{\partial r}\left(r\frac{\partial T}{\partial r}\right), \tag{3.5}$$

with boundary conditions $T|_{r=a} = T_S$, $T|_{x=0} = T_i$, $\frac{\partial T}{\partial r}\big|_{r=0} = 0$.
It is more convenient to solve this by defining a new variable $\eta = r/a$, which scales the radial coordinate by the radius of the tube, so that streamlines of the flow are lines of constant η. Under this transformation equation (3.5) becomes

$$\frac{2Q}{\kappa\pi a^2}(1-\eta^2)\frac{\partial T}{\partial x} = \frac{1}{a^2}\frac{1}{\eta}\frac{\partial}{\partial \eta}\left(\eta\frac{\partial T}{\partial \eta}\right) \tag{3.6}$$

with boundary conditions $T|_{\eta=1} = T_s$, $\frac{\partial T}{\partial \eta}\Big|_{\eta=0} = 0$, $T|_{x=0} = T_i$.

The final equation is for the radius. The time-dependent equation for the radius is a standard Stefan equation (e.g. [18])

$$\frac{L_H}{c_p}\frac{\partial a}{\partial t} = \kappa\left(\frac{\partial T_e}{\partial r}\bigg|_{r=a} - \frac{\partial T}{\partial r}\bigg|_{r=a}\right), \tag{3.7}$$

where κ is thermal diffusivity of both the liquid and the solid, which are assumed here to be equal in magnitude, L_H is the latent heat of solidification, and c_p is the heat capacity of the liquid. The rate of change of the radius of the tube is proportional to the difference in heat flux at the boundary of the tube, which, by the slowly-varying-in-x assumption, is the flux in the radial direction only.

3.2. Steady-state solutions

We first consider the solution for the steady state of the model, given by the steady components of (3.1), (3.3), (3.6) and (3.7) with the corresponding boundary conditions. The equations are non-dimensionalized with $x = L\chi$, $a = r_0\alpha$, $\frac{T-T_s}{T_i-T_s} = \theta$, $\frac{T_e-T_s}{T_i-T_s} = \theta_e$, $Q = \frac{\kappa L\pi}{2}q$, $P = \frac{4\mu\kappa L^2}{r_0^4}p$, and $u = \frac{\kappa L}{r_0^2}u'$. Pressure is non-dimensionalized so it remains in the balance to first order, and flux is non-dimensionalized so that the effect of conductive cooling is balanced by advection. The model depends on a dimensionless imposed temperature difference

$$T_n = \frac{T_s - T_0}{T_i - T_S}. \tag{3.8}$$

The non-dimensional velocity and the temperature in the solid are

$$u' = \frac{q}{\alpha^2}\left(1-\eta^2\right), \qquad \theta_e = \frac{T_n\ln\eta}{\ln\alpha} \quad (\eta \geq 1) \tag{3.9}$$

and the pressure drop across the tube Δp is related to the flux by:

$$\Delta p = q\int_0^1 \frac{1}{\alpha^4}\mathrm{d}\chi. \tag{3.10}$$

The steady non-dimensional internal temperature equation is

$$q(1-\eta^2)\frac{\partial\theta}{\partial\chi} = \frac{1}{\eta}\frac{\partial}{\partial\eta}\left(\eta\frac{\partial\theta}{\partial\eta}\right). \tag{3.11}$$

This can be solved by separation of variables to give

$$\theta(\chi,\eta) = \sum_n A_n \mathrm{e}^{-\lambda_n^2\chi/q}\phi_n(\eta), \tag{3.12}$$

where λ_n, ϕ_n are the eigenvalues and eigenfunctions of the problem $\frac{1}{\eta}\frac{\partial}{\partial\eta}(\eta\frac{\partial\phi_n}{\partial\eta}) + \lambda_n^2(1-\eta^2)\phi_n = 0, \phi_n(0) = 1, \phi_n(1) = 0, \phi_n'(0) = 0$. The solution was originally found by Graetz [19] for flow of uniform viscosity through a pipe of constant radius, and was modified for steady flow with solidification as in this configuration by Zerkle and Sunderland [8]. The A_n are constants determined from the upstream temperature distribution. A more complete discussion of this solution, including numerical values, is given in the appendix of [3]. In steady state, the dimensionless equation at the liquid solid interface becomes

$$\frac{\partial\theta}{\partial\eta}\bigg|_{\eta=1} = \frac{\partial\theta_e}{\partial\eta}\bigg|_{\eta=1}. \tag{3.13}$$

Using (3.9) and (3.12), we calculate

$$\frac{\partial\theta_e}{\partial\eta}\bigg|_{\eta=1} = \frac{T_n}{\ln\alpha},$$

$$\frac{\partial\theta}{\partial\eta}\bigg|_{\eta=1} = \sum G_n \mathrm{e}^{-\lambda_n^2\chi/q}, \quad \text{where } G_n = A_n\frac{\partial\phi_n}{\partial\eta}\bigg|_{\eta=1},$$

so the radius of a steady-state tube is

$$\alpha(\chi) = \exp\left(\frac{T_n}{\sum G_n \mathrm{e}^{-\lambda_n^2\chi/q}}\right). \tag{3.14}$$

Profiles of α for several different values of q are shown in Fig. 5a. Note the relation between α, q, and Δp. If flux q is prescribed then (3.14) gives an explicit solution for α, while if Δp is prescribed it must be solved in conjunction with (3.10), which provides a transcendental integro-differential equation for α. Fig. 6a shows the pressure drop as a function of flux for a steady-state tube, for a particular choice of temperature constant. This has a minimum

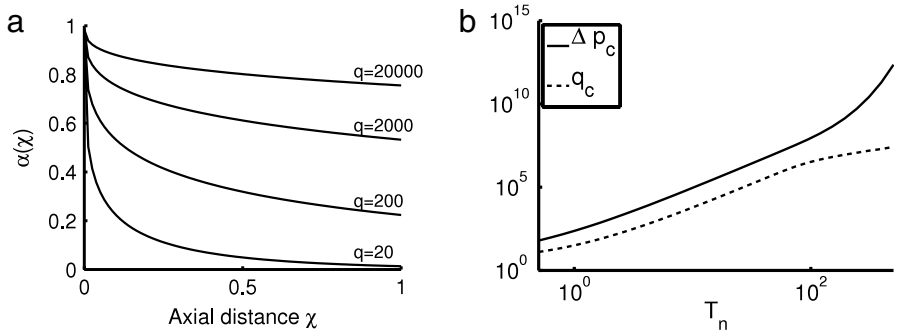

Fig. 5. (a) Steady-state curves of shape of the tube $\alpha(\chi)$ for several different values of flux q. (Note that these curves are obtained from one another by re-scaling χ.) The top two curves are stable at fixed pressure drop, and the bottom two curves are unstable. (b) Critical pressure drop Δp_c (solid) and critical flux q_c (dashed) as a function of non-dimensional temperature constant T_n.

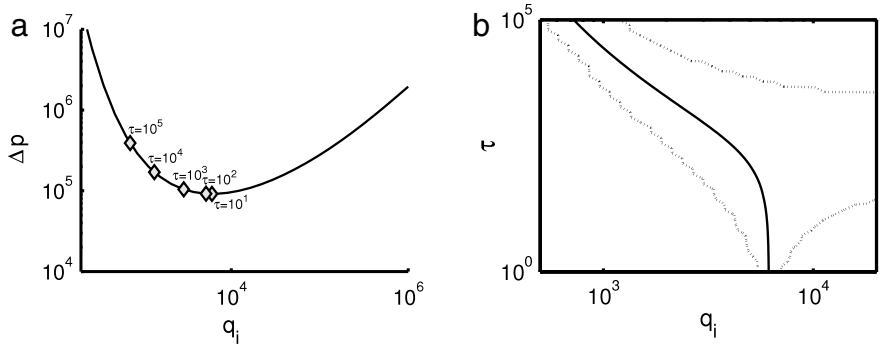

Fig. 6. (a) Pressure drop Δp of a steady-state tube with flux q_i. When $\tau = 0$ (constant pressure drop), all tubes on the right-hand branch are stable and all tubes on the left-hand branch are unstable. As τ increases, the transition to instability moves leftwards, so that more profiles are stable. Markers indicate the critical value of flux above which the system becomes stable for a given fixed τ. (b) Stability regions for linear perturbation problem, as a function of q_i and τ. The solid line marks the boundary between stability (right) and instability (left). The region between the dashed lines has complex eigenvalues, so the perturbed equations show oscillating solutions. The temperature constant for both figures is $T_n = 10$.

Δp_c at a critical flux q_c, suggesting that when $\Delta p > \Delta p_c$ there are two solutions for a steady-state tube and when $\Delta p < \Delta p_c$ there are no possible tubes, a fact which has been verified analytically in [20]. The critical pressure drop $\Delta p_c(T_n)$ and critical flux at which it is attained $q_c(T_n)$ are shown in Fig. 5b.

Note the qualitative similarities between the analytic pressure-drop–flux relationship in Fig. 6a and the experimental results in Fig. 3: as flux is decreased there is a very weak decline in pressure drop, and then a sudden sharp increase for low values of flux.

3.3. Linear stability analysis

To investigate stability we introduce an upstream condition with an additional parameter to capture each of the three possibilities: (i) constant flux, (ii) constant pressure, and (iii) a model allowing the two variables to co-vary. One assumes that the tube is fed from an upstream reservoir that in turn is fed by a steady volume flux of rate Q_i. (The model can also be derived by assuming that the upstream reservoir is elastic.) Flow from the reservoir obeys the equation

$$A\frac{\mathrm{d}H}{\mathrm{d}t} = Q_i - Q,$$

where A is the cross-sectional area of the reservoir and H is the fluid elevation in it. The downstream end of the tube is open and hence at atmospheric pressure, so the pressure drop across the tube is given by

$$\Delta P = g\rho H.$$

Letting the timescale be Sr_0^2/κ, where the Stefan number is $S = L_H/c_p\,(T_i - T_S)$, and non-dimensionalizing the other scales as before, leads to the non-dimensional system

$$\frac{\partial\alpha}{\partial t} = \frac{1}{\alpha}\left(E(\alpha) - I(\chi, q)\right) \tag{3.15a}$$

$$\frac{\mathrm{d}\Delta p}{\mathrm{d}t} = \tau\,(q_i - q) \tag{3.15b}$$

$$\Delta p = q\int_0^1 \frac{1}{\alpha^4}\mathrm{d}\chi \tag{3.15c}$$

where the temperature gradient in the solid at the solid–liquid interface is $E(\alpha) = \left.\frac{\partial\theta_e}{\partial\eta}\right|_{\eta=1} = \frac{T_n}{\ln\alpha}$, and the temperature gradient in the liquid at the interface is $I(\chi, q) = \left.\frac{\partial\theta}{\partial\eta}\right|_{\eta=1} = \sum G_n \mathrm{e}^{-\lambda_n^2\chi/q}$. This model has a new non-dimensional parameter $\tau = \frac{\pi g S r_0^6}{8A\nu\kappa L}$, which measures the rate of change of the upstream pressure relative to the rate of change of the radius of the interface, and is proportional to the Stefan number times a thermal response time r_0^2/κ divided by the hydraulic reservoir response time $AL\nu/gr_0^4$. The latter is the exponential time for a viscous fluid to empty the reservoir with no solidification ($T_n \to 0$).

The model also depends on the non-dimensional flux q_i into the upstream reservoir. Therefore, the dynamics of (3.15) are determined by the three parameters T_n, τ, q_i. When $\tau = 1$, the elevation, or pressure in the reservoir adjusts extremely slowly to changes in the flux, and by extension the radius of the tube, so the system should behave as if the pressure drop were held constant, with a constant pressure drop system recovered exactly when $\tau = 0$. When $\tau \gg 1$, the pressure in the reservoir adjusts rapidly to the flux into the reservoir so the system should behave as if the flux through the tube were held constant. Thus, setting different values

Table 2
Particular form of the functions used in the perturbation calculations.

$E(\alpha(\chi,t)) = \frac{\partial\theta_c}{\partial\eta} = \frac{T_n}{\ln\alpha}$
$I(\chi,q) = \frac{\partial\theta}{\partial\eta} = \sum G_n e^{-\lambda_n^2\chi/q}$
$E_\alpha(\chi) \equiv \frac{1}{\alpha_0}\frac{dE}{d\alpha}\big|_{\alpha_0} = \frac{-T_n}{\alpha_0^2(\ln\alpha_0)^2}$
$P_q \equiv \frac{\partial\Delta p}{\partial q}\big|_{\alpha_0,q_0} = \int_0^1 \frac{1}{\alpha_0^4}d\chi$
$P_\alpha[\alpha_1] \equiv \frac{\delta\Delta p}{\delta\alpha}\big|_{\alpha_0,q_0}[\alpha_1] = q_i\int_0^1 \frac{-4\alpha_1}{\alpha_0^5}d\chi$
$A_q \equiv \frac{\partial\alpha_0}{\partial q}\big|_{q_0} = \alpha_0\frac{T_n}{\left(\sum G_n e^{-\lambda^2\chi/q_i}\right)^2}\sum G_n\frac{\lambda_n^2\chi}{q_i^2}e^{-\lambda^2\chi/q_i}$

of τ allows us to quantitatively interpolate between constant flux and constant pressure drop conditions.

Let us now examine the linear stability of (3.15). Expanding up to first order in small ε, $q = q_0 + \varepsilon q_1$, $\alpha = \alpha_0 + \varepsilon\alpha_1$ and $\Delta p = p_0 + \varepsilon p_1$ (note that we have dropped the Δ symbol for the pressure drop steady states and perturbations), the steady state is

$$q_0 = q_i \tag{3.16a}$$

$$\alpha_0 = \alpha_0(\chi, q_i) = \exp\left(\frac{T_n}{\sum G_n e^{-\lambda_n^2\chi/q_i}}\right) \tag{3.16b}$$

$$p_0 = q_i\int_0^1 \frac{1}{\alpha_0^4}d\chi \tag{3.16c}$$

and the $O(\varepsilon)$ parts are

$$\frac{\partial\alpha_1}{\partial t} = \frac{1}{\alpha_0}\left(\frac{dE}{d\alpha}\Big|_{\alpha_0}\alpha_1 - \frac{\partial I}{\partial q}\Big|_{q_0}q_1\right) \tag{3.17a}$$

$$\frac{dp_1}{dt} = -\tau q_1 \tag{3.17b}$$

$$q_1 = \frac{p_1 - \frac{\delta\Delta p}{\delta\alpha}\big|_{\alpha_0,q_0}[\alpha_1]}{\frac{\partial\Delta p}{\partial q}\big|_{\alpha_0,q_0}}. \tag{3.17c}$$

The forms of some of the functions are given in Table 2. In these equations we have taken care to distinguish between partial derivatives and functional derivatives, by using the symbol ∂ for a partial derivative and δ for a functional derivative, which results in a linear operator. We simplify notation by writing $E_\alpha(\chi) \equiv \frac{1}{\alpha_0}\frac{dE}{d\alpha}\big|_{\alpha_0}$. Let us analyze the three different boundary conditions in turn.

Case (i) *Constant flux.* The stability of the constant flux case is simple to analyze separately. Replacing (3.17b) with the condition $q_1 = 0$ and substituting for $E(\alpha)$, Eq. (3.17a) becomes

$$\frac{d\alpha_1}{dt} = E_\alpha\alpha_1 = \frac{-T_n\alpha_1}{\alpha_0^2\ln^2\alpha_0}.$$

Since both $\alpha_0, T_n > 0$, we have that $sgn(d\alpha_1/dt) = -sgn(\alpha_1)$ for every χ, so this equation is sign-definite and hence linearly stable.

Case (ii) *Constant pressure.* This case was first analyzed by Sampson and Gibson [13]. Recall that for a given pressure drop there are two possible steady-state tubes, one with $q > q_c$ and one with $q < q_c$, where q_c is the value of flux which minimizes pressure drop. By computing the single eigenvalue in the discrete spectrum of the operator on the right-hand side of (3.17), Sampson and Gibson showed that only the former is linearly stable. Holmes [20] analyzed this case in more detail by considering the full spectrum of the operator, obtaining the same results for the discrete spectrum and further showing that the continuous spectrum is exactly Range$\{E_\alpha\} = (-\infty, c)$ where $c < 0$, so that only the discrete spectrum determines the stability properties.

Case (iii) *Variable pressure and flux.* This case is considerably more difficult to analyze analytically, and we will ultimately rely on numerical results. These show that as in the constant pressure case, the continuous spectrum appears to be Range$\{E_\alpha\}$ which is entirely negative, so we focus our analysis on the discrete spectrum.

Returning to (3.17), the equations can be rewritten by noting that α_0 solves the equation $E(\alpha_0(q,\chi)) = I(q,\chi)$, so taking the partial q-derivative and evaluating at q_0 gives $\frac{\partial I}{\partial q}\big|_{q_0} = \frac{dE}{d\alpha}\big|_{\alpha_0}\frac{\partial\alpha_0}{\partial q}\big|_{q_0}$. Here we introduce symbols $A_q, P_q, P_\alpha[\alpha_1]$ to represent the derivative terms, which are defined precisely in Table 2. Under these transformations, (3.17a) and (3.17b) become

$$\frac{d\alpha_1}{dt} = E_\alpha\left(\alpha_1 - \frac{p_1 - P_\alpha[\alpha_1]}{P_q}A_q\right)$$
$$\frac{dp_1}{dt} = \frac{-\tau}{P_q}\left(p_1 - P_\alpha[\alpha_1]\right).$$

To find the eigenvalues in the discrete spectrum, we look for a solution of the form $(\alpha_1, p_1) = e^{\lambda t}(\tilde\alpha_1, \tilde p_1)$, substitute into the above equations, and solve to get

$$\tilde p_1 = \frac{\tau P_\alpha[\tilde\alpha_1]}{(P_q\lambda + \tau)} \tag{3.18}$$

$$\tilde\alpha_1 = \frac{-E_\alpha(\tilde p_1 - P_\alpha[\tilde\alpha_1])A_q}{P_q(\lambda - E_\alpha)} = \frac{P_\alpha[\tilde\alpha_1]E_\alpha A_q\lambda}{(P_q\lambda + \tau)(\lambda - E_\alpha)}. \tag{3.19}$$

These equations are valid provided $\lambda \neq -\tau/P_q$ and $\lambda \neq E_\alpha(\chi)$ $\forall\chi$. The first is a single point, which can be ignored. The second exception requires $\lambda > \max_\chi(E_\alpha(\chi))$, which is simply the condition that λ is greater than the supremum of the continuous spectrum, which again we denote by c. Therefore, we consider (3.18) and (3.19) only for $\lambda \in (c,\infty)\setminus\{-\tau/P_q\}$.

Applying the operator P_α to (3.19) leads to an equation for λ:

$$F(\lambda) \equiv P_\alpha\left[\frac{E_\alpha A_q\lambda}{(P_q\lambda + \tau)(\lambda - E_\alpha)}\right] - 1 = 0. \tag{3.20}$$

If $\tau = 0$ this equation is exactly the constant pressure case mentioned above. For other values of τ we solved this equation numerically for λ in (q_i, τ) parameter space. The full regions of stability/instability and oscillating solutions for a representative value of dimensionless temperature constant $T_n = 10$ are summarized in Fig. 6b. Let us describe these in more detail.

Consider a fixed q_0 such that it is less than the flux q_c that minimizes pressure drop. If $\tau = 0$ there is one eigenvalue, and the tube is unstable. As τ increases, there is a critical value of τ at which a bifurcation occurs and the system has three eigenvalues. One of these is real and the other two are complex with non-zero imaginary parts. The real root is always negative and less than $-\tau/P_q$, so we track the signs of the complex roots in order to detect instability. As τ increases, the real parts of the roots decrease, eventually crossing zero so that the system becomes stable. As τ is further increased, the complex eigenvalues eventually disappear.

For $q_0 > q_c$ the system is always stable. As τ increases, a similar bifurcation occurs, with complex eigenvalues appearing for large τ and disappearing for even larger τ. For a fixed value of τ, this means that there is a critical value of q_0 below which the system is unstable, and above which the system is stable. This critical value is plotted with diamonds in Fig. 6a for several values of τ. The figure shows that the critical value decreases as τ increases, so that the range of stable steady states is much greater with large τ. As $\tau\to\infty$, all steady states become stable, corresponding to case (i) with constant flux. As anticipated, the value of τ serves the function of interpolating between constant pressure drop and constant flux for quantifying a stability criterion.

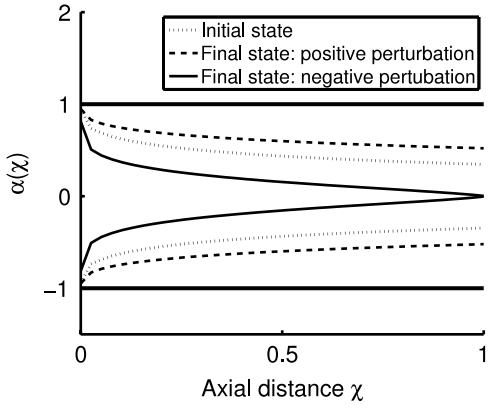

Fig. 7. Final states of two numerical simulations done at fixed pressure drop. The simulation was started with the unstable profile (dotted line) corresponding to a flux of 3×10^3, and a small perturbation of either $+0.01$ or -0.01 was added to the profile. For the positive perturbation, the tube opens up and moves to the stable steady-state profile corresponding to the same value of pressure (dashed line). The final flux is 1.38×10^4. For the negative perturbation, the tube freezes shut (solid line).

3.4. Numerical simulations of stability

Numerical simulations of the non-dimensional equations (3.15) were performed to test the linear stability predictions. The pressure difference was either kept constant, or varied according to (3.15b), and the tube radius was stepped forward in time using (3.15a). Time derivatives were calculated using forward Euler, the trapezoidal rule was used for integration, and 1000 eigenvalues were used to calculate the heat flux and steady profiles. 40 points were used to represent the tube in the horizontal direction. The simulations were stopped if the tube froze shut, i.e. when $\alpha(\chi, t) = 0$ for some χ. The numerical simulations confirm the theoretical predictions. Small perturbations to a profile that is linearly stable return to the original state, whereas perturbations to a profile which is linearly unstable eventually freeze shut for $\tau \neq 0$. The perturbation oscillates about the steady state as it grows or decays exactly where linear theory predicts complex eigenvalues.

Consider now the fixed pressure case, $\tau = 0$, which is unique as it has two possible steady states, one stable and the other unstable. Fig. 7 shows the two different types of evolution that are possible if we start with the linearly unstable profile and perturb it a little. If the perturbation is mostly positive, in the direction of the stable profile corresponding to the same value of Δp, then the tube opens up, and moves to the stable profile. If the perturbation is mostly negative, away from the stable profile, then the tube freezes shut. As the tube moves from one profile to another, its shape is always close to that of a steady profile. Any localized disturbances to the profile are rapidly ironed out. This is consistent with the linear theory, which predicts large negative eigenvalues in the continuous spectrum that appear to be associated with highly localized eigenfunctions.

Fig. 8 shows two cases of the radius at the endpoint of the tube $\alpha(1)$ in the case of a growing or decaying oscillating solution. The time constant τ was kept constant, and the flux varied so that it was to the right of the critical flux in one case, and to the left in the other. In the first case, a small perturbation oscillated about the steady state and eventually decayed, leaving a steady-state tube in its wake. In the second case, a small perturbation oscillated about the steady state but grew larger, and eventually the tube froze shut.

3.5. Application: length of a lava tube

One motivation for this study was to explain the length of lava tubes observed in some volcanic flows on Earth and Mars, where tubes of 50–200 km have been found [3]. Such steady-state tubes, which are formed when highly viscous lava flows down low-angle slopes, often terminate because of geographical features such as an abrupt change in slope or reaching an ocean, and it would be interesting to know whether there are physical constraints governing their lengths as well. Therefore, as a final note, we would like to show some simple calculations to illustrate how this model can be used to provide an upper bound for the length of a melt conduit in an Earth or planetary context. In many tubes, the pressure at the upstream end of the tube is dominated by the hydrostatic pressure so we use this as the constraint. Recalling that the non-dimensional pressure drop must be greater than a critical value in order for a steady-state tube to exist, the length satisfies

$$\frac{\Delta P r_0^4}{4\kappa\mu L^2} \geq \Delta p_c(T_n) \Leftrightarrow L \leq \sqrt{\frac{\Delta P r_0^4}{4\kappa\mu\Delta p_c(T_n)}}. \tag{3.21}$$

Using typical lava parameters [21,3] $\kappa = 10^{-7}$ m^2/s, $\rho = 2300$ kg/m^3, $\mu = 60(54\text{–}160)$Pa $\cdot$ s , $T_i = 1133\text{–}1187$ °C, $T_s = 1077$ °C, $T_0 = 30$ °C, (these temperatures correspond to $T_n = 8\text{–}20$), and calculating the hydrostatic pressure difference as $\Delta P = \rho g H$, where H is the total vertical distance traveled by the lava tube and g is gravity, we find that a tube with a radius of 10 m which drops 1 km can have a maximum length of 110–440 km.

It is encouraging that this is consistent with observations, but we note that there are many reasons (not detailed here) why this model is too idealized to make direct conclusions about lava tubes. We note also that our mixed upstream condition applies in certain flows, such as when the lava tube drains from a lava lake or an interior elastic magma chamber, each receiving lava either steadily or impulsively from a source inside the earth, in which case the linearized version of the geophysical upstream condition is similar

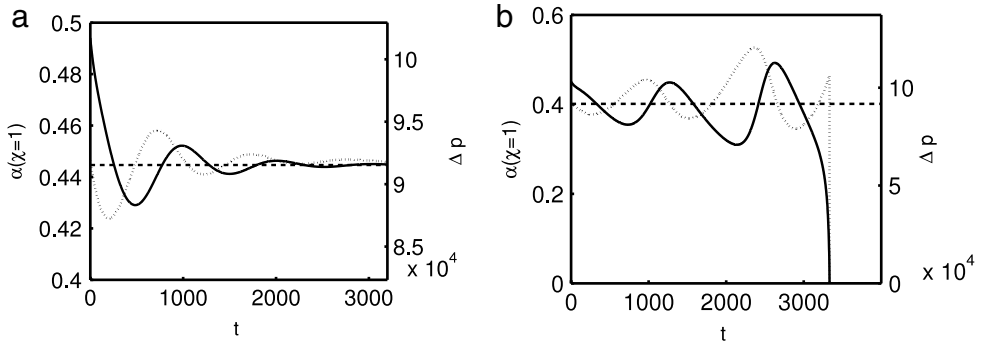

Fig. 8. Radius at the end point (solid curve, left axis) and pressure drop across the tube, (dotted line, right axis) for (a) stable flow and (b) unstable flow. The steady states for both variables coincide. (a) Stable oscillation, with $q_i = 7 \times 10^3$. Tube eventually moves to steady state. (b) Unstable oscillation, with $q_i = 5 \times 10^3$. The perturbation grows larger as it oscillates and eventually the tube freezes shut. The parameters for both simulations are $T_n = 10$, $\tau = 100$.

to (3.15b). However, due to the difficulty of obtaining accurate data for such flows we prefer not to speculate on numerical values at present.

4. Summary and discussion

We conducted a laboratory experiment which shows that when fluid flows through a tube whose boundary is held below freezing, solid material forms on the boundary, leaving an inner tube of flowing liquid. As the flow rate is progressively decreased, the pressure drop across the tube first decreases and then increases before finally the tube freezes shut.

We investigate a theoretical model for low Reynolds number flow through a tube with solidification, in which we solve for the shape of a steady-state tube as a function of distance downstream and find the relationship between pressure drop and flux in steady state. This shows that the pressure drop has a minimum as flux is varied. The linear stability of the steady states depend on the upstream boundary condition: when constant flux is applied, all states are predicted to be stable; when constant pressure drop is applied, those corresponding to a flux less than the flux at the minimum are unstable, and for a coupled condition the critical flux for stability is in between. In the experiments, pressure drop and flux were coupled by the measuring device, so these qualitative results may explain the experimental rise in pressure drop as flux is slowly decreased to freezing value.

Attempts to produce a full quantitative comparison between the laboratory experiment and the theory have produced poor results which we attribute to numerous possible causes of uncertainty in the experiment. There was, of course, uncertainty in the mean values as well as internal variations of viscosity and specific heat, which makes quantitative comparison difficult. There is also an overall sensitivity of the system to the precise tube geometry, which is not captured by an axisymmetric model. Our experiments showed that small perturbations near the endpoint could initiate large-scale freezing events. Most solidifying materials have some crystal structure that might generate local flaws, and even small bits of foreign material (particles, dust, microbubbles, etc.) might produce effects that get magnified near the exit. It is possible that experiments using pure filtered or distilled water that is completely free of dust, particles and dissolved air, could produce results much closer to theory since it has very well-known material properties and minor viscosity changes near freezing. However, it is important to note again that the earlier experiments with water (e.g. [8–11]) exhibited wave formation in the ice and that such local features might be common and that their role in freeze-up is probably not yet fully appreciated. To clarify such points, optical views of the liquid tube interiors would be very useful.

Overall, our findings suggest that the distance traveled by fluid in a melt conduit is very sensitive to the conditions that govern pressure and flow rate at the upstream end. One of our motivations was to study the paths of magma and lava flows, which are well known to be quite complicated. We suggest that the sensitive interrelation between upstream pressure and the stability of the tube at the downstream end, where it is most likely to freeze shut, is one mechanism responsible for such complexity.

Acknowledgements

Support was received from the Geophysical Fluid Dynamics Program, which is supported by the Ocean Sciences Division of the National Science Foundation under Grant OCE-0325296, and from the Oceanography Section of the Office of Naval Research under Grant N00014-07-1-0776. The laboratory experiments were supported by the Deep Ocean Exploration Institute of W.H.O.I. M.C. Holmes-Cerfon would like to thank Lou Howard for many helpful conversations during the GFD summer program. We are also very grateful for the thorough help and comments of two anonymous referees.

References

[1] P.M. Bruce, H.E. Huppert, Thermal control of basaltic fissure eruptions, Nature 342 (1989) 665–667.
[2] P.M. Bruce, H.E. Huppert, Solidification and melting in dykes by the laminar flow of basaltic magma, in: M.P. Ryan (Ed.), Magma Transport and Storage, Wiley, New York, 1990, pp. 87–102. 420 pp.
[3] S.E.H. Sakimoto, M.T. Zuber, Flow and convective cooling lava tubes, J. Geophys. Res. 103 (1998) 27465–27487.
[4] M. Dragoni, F. Donza, A. Tallarico, Temperature distribution inside and around a lava tube, J. Volcanol. Geotherm. Res. 115 (2002) 43–51.
[5] S.E.H. Sakimoto, T.K.P. Gregg, Channeled flow: analytic solutions, laboratory experiments, and applications to lava flows, J. Geophys. Res. 106 (2001) 8629–8644.
[6] F. Klingelhofer, M. Hort, H.J. Kumpel, H.U. Schmincke, Constraints on the formation of submarine lava flows from numerical model calculations, J. Volcanol. Geotherm. Res. 92 (1999) 215–229.
[7] J. Lister, P. Dellar, Solidification of pressure-driven flow in a finite rigid channel with applications to volcanic eruptions, J. Fluid Mech. 323 (1996) 267–283.
[8] R.D. Zerkle, J.E. Sunderland, The effect of liquid solidification in a tube upon laminar-flow heat transfer and pressure drop, Trans. ASME C 90 (1968) 183–190.
[9] J.C. Mulligan, D.D. Jones, Experiments on heat transfer and pressure drop in a horizontal tube with internal solidification, Int. J. Heat Mass Transfer 19 (1976) 213–219.
[10] T Hirata, M. Ishihara, Freeze-off conditions of a pipe containing a flow of water, Int. J Heat Mass. Trans. 28 (2) (1985) 331–337.
[11] B. Weigand, J. Braun, S.O. Neumann, K.J. Rinck, Freezing in forced convection flows inside ducts: a review, Heat Mass Transfer 32 (1997) 341–351.
[12] D.G. Lee, R.D. Zerkle, The effect of liquid solidification in a parallel plate channel upon laminar-flow heat transfer and pressure drop, J. Heat Transfer 91 (1969) 583–585.
[13] P. Sampson, R.D. Gibson, A mathematical model of nozzle blockage by freezing, Int J. Heat Mass Transfer 24 (1981) 231–241.
[14] S.M. Richardson, Injection moulding of thermoplastics: freezing of at gates, Rheol. Acta 24 (1985) 497–508.
[15] M. Epstein, F.G. Chueng, Complex freezing–melting interfaces in fluid flow, Ann. Rev. Fluid Mech. 15 (1983) 293.
[16] S.M. Richardson, Injection moulding of thermoplastics: freezing of variable-viscosity fluids. III Fully developed flows, Rheol. Acta 25 (1986) 372–379.
[17] C.V. Bindhu, S.S. Harilal, V.P.N. Nampoori, C.P.G. Vallabhan, Thermal diffusivity measurements in organic liquids using transient thermal lens calorimetry, Opt. Eng. 37 (10) (1998) 2791–2794.
[18] D.L. Turcotte, G. Schubert, Geodynamics, Cambridge University Press, 2002, 482 pp.
[19] L. Graetz, Uber die Wärmeleitungsfähigkeit von Flüssigkeiten, Ann. Phys. Chem. 18 (1883) 79.
[20] M. Holmes, Length and shape of a lava tube, in: Woods Hole Oceanographic Institution Geophysical Fluid Dynamics Program Proceedings Volume 2007, 2007. http://www.whoi.edu/page.do?pid=19276.
[21] L.P. Keszthelyi, Emplacement of the 75-km-long Carrizozo lava flow field, south-central New Mexico, J. Volcanol. Geotherm. Res. 59 (1993) 59–75.